International Journal of Nanomedicine

Dovepress
open access to scientific and medical research

Open Access Full Text Article

ORIGINAL RESEARCH

Proof of Concept of the Radiosensitizing Effect of Gadolinium Oxide Nanoparticles in Cell Spheroids and a Tumor-Implanted Murine Model of Chondrosarcoma

Marie-Thérèse Aloy[1,*], Jacqueline Sidi Boumedine[2,*], Agathe Deville[2,3], David Kryza[2], Arnaud Gauthier[1,4], Delphine Brichart-Vernos[1,5], Grégoire Ollier[1], Veronica La Padula[5], François Lux[5], Olivier Tillement[5], Claire Rodriguez-Lafrasse[1,4,*], Marc Janier[2,3,*]

[1]Laboratory of Cellular and Molecular Radiobiology, UMR CNRS5822/IP2I, Lyon-Sud Medical School, Univ Lyon, Lyon 1 University, Oullins, France; [2]CNRS, LAGEPP, UMR5007, IMTHERNAT, Lyon 1 University, Hospital Edouard Herriot, Lyon, France; [3]Department of Nuclear Medicine, Groupement Hospitalier Est, Hospices Civils de Lyon, Lyon, France; [4]Department of Biochemistry and Molecular Biology, Groupement Hospitalier Sud, Hospices Civils de Lyon, Pierre-Bénite, France; [5]Light Matter Institut UMR CNRS 5306, Lyon 1 University, Villeurbanne, France

*These authors contributed equally to this work

Correspondence: Marc Janier, Department of Nuclear Medicine, Groupement Hospitalier Est, Hospices Civils de Lyon, Lyon, 69634, France, Tel +33472356999, Fax +33472357345, Email marc.janier@univ-lyon1.fr

Purpose: Chondrosarcomas (CHSs), which represent 20% of primary bone tumors in adults, are mostly resistant to radio- and chemotherapy. It is therefore essential that new therapeutic approaches, targeted to the tumour, be developed to improve the prognosis of patients. The effectiveness, as a radiosensitizing agent, of gadolinium oxide nanoparticles (GdoNP, AGuIX®) nanoparticles in CHS was evaluated in vitro, in spheroid CHS models allowing to reproduce cell-cell extracellular matrix interactions, and, in vivo, in a nude mouse model with heterotopic tumour xenograft.

Methods: Spheroids from SW1353 and HEMC-SS cells were characterized by confocal microscopy with or without GdoNP treatment. Real-time microscopy enabled quantification of cell viability, cell migration and invasion. In vivo, the efficacy of the association of GdoNP combined with a single (4Gy) or fractionated (4x1Gy) irradiation was evaluated in HEMC-SS tumor-bearing mice by monitoring tumor growth, mouse survival and gene expression profile.

Results: The expression of proteoglycans in the extra-cellular matrix (ECM) of spheroids demonstrated the relevance of the 3-D model. The combination of GdoNP with single or fractionated irradiation increased the lethal effects of irradiation on 2-D- and 3-D-cultured cells. In vivo, a single or a fractionated dose of 4 Gy associated with IT or IV injection of GdoNP decreased tumor growth significantly. Only IT injection increased mice survival. Unexpectedly, the radiosensitizing effect of GdoNP was associated, in vitro, with a significant decrease in invasion-migration capacities and, in vivo, with the decreased expression of PTX3, a protein involved in the epithelial-to-mesenchymal transition process, suggesting a potential impact of GdoNP on metastasis formation.

Conclusion: These results provide the first proof of concept of the radiosensitizing effect of GdoNP in CHSs and opened the way for a multicentre, randomized Phase 2 trial evaluating the association of GdoNP with radiotherapy for the therapeutic management of patients with symptomatic inoperable musculoskeletal tumor lesions.

Keywords: chondrosarcoma, AGuIX® nanoparticle, radiosensitization, PTX3

Introduction

Chondrosarcoma (CHS) is the second most common primary bone sarcoma in humans after osteosarcoma. Almost 90% of CHSs are of the conventional subtype. They are characterized by the production of a hyaline cartilage matrix, with poor vascularization and are usually found in the medulla or at the surface of the bone.[1] Extra-skeletal myxoid

Received: 16 September 2022
Accepted: 9 December 2022
Published: 23 December 2022

chondrosarcoma (EM-CHS) is a rare mesenchymal neoplasm of uncertain differentiation that arises mostly in the deep soft tissue of the proximal extremities and limb girdles, with a tendency for local or distant recurrence, usually located in lungs.[2,3] EM-CHS differs from conventional CHS by its site occurrence, expression of differentiation markers and genetic characteristics. All CHS subtypes are characterized by their resistance to radio- and chemotherapy due to specific hallmarks.[1,4,5] Like hyaline cartilage, tumor tissue is characterized by a dense and extensive extra-cellular matrix (ECM) that creates a semipermeable physical barrier. This barrier reduces blood flow, creating severe chronic cellular hypoxia, and limits access of cytotoxic agents with a resulting resistance to therapies.[6,7]

Surgery remains the main therapeutic approach for CHS with potential dramatic excision and amputation because the local control of the tumor is of paramount importance to prevent future metastases. For inoperable or incompletely resected tumors, high-dose radiation therapy (RT) is indicated.[8–10] Despite these different strategies of treatment, the 5-year survival rate is lower than 50% for grade III patients[5] and 70% will develop metastases.[8] Finding a more efficient treatment to prevent the recurrence of CHS and metastasis formation is thus a considerable challenge. Therefore, overcoming radioresistance and increasing the dose delivery within these tumors during RT seems to be of interest.

A promising therapeutic strategy results from the combination of photon irradiation with nanoparticles containing high-Z elements such as gold, hafnium or gadolinium.[11–13] Because of their high atomic number, they amplify the effects of radiation by producing high levels of ionization and secondary electrons leading to the generation of reactive oxygen species (ROS).[14] Our group, and others, have successively demonstrated the radiosensitizing effects of Gadolinium oxide nanoparticles (AGuIX®, NH TherAguix, Meylan, France) (GdoNP), in different cellular and animal tumor models.[15–18] The proof of concept in melanoma brain metastases[19] led to the first-in-man clinical trial (NCT 02820454: NANORAD 1) in multiple brain metastases. Based on the promising results of this clinical study,[20] clinical studies combining GdoNP with radiotherapy were extended to other tumor localizations: cervical cancer (NANOCOL, NCT03308604), glioblastoma (NANO-GBM, NCT 04881032), and lung and pancreatic cancers (Nano-SMART, NCT04789486). In the present work, in view of extending GdoNP clinical indication to CHSs, we propose a preclinical proof of concept of their radiosensitizing properties in two different subtypes of human CHS cell lines (HEMC-SS, an EM-CHS and SW1353, a conventional CHS), maintained in 2-D and 3-D cultures, as well as in a model of a nude mouse bearing HEMC-SS xenografts irradiated with photons after intratumoral (IT) or intravenous (IV) injection of NPs. Unexpectedly, we also demonstrated a new property of GdoNP related to the inhibition of cell migration and invasion processes.

Materials and Methods

2-D Cell Culture

The human EM-CHS cell line HEMC-SS, derived from the muscle of a 77-year-old female with lymph node and lung metastases, was obtained from the European Collection of Animal Cell Cultures (ECACC, Salisbury, UK). The human SW1353 CHS cell line, derived from a primary grade II CHS of the humerus, was purchased from CellSystems (Troisdorf, Germany). They were both cultured in a monolayer in DMEM/F12–Glutamax–0.5 mM sodium pyruvate media (Gibco, Bedford, MA, USA), supplemented with 10% fetal calf serum (FCS, Dutscher, Brumath, France), 4 mg/L gentamicin (Sigma Aldrich, St Quentin Fallavier, France) and maintained at 37 °C under 5% CO_2.

3-D Culture

To generate spheroids, cells were trypsinized and seeded at 2000 cells for HEMC-SS and 4000 cells for SW1353 cells in Ultra-Low Attachment round-bottom 96-well plates (ULA, Corning, Acton, MA, USA) containing 100 µL of chondrogenic medium consisting of DMEM/F12 supplemented with 1% FCS, 4 g/L gentamicin, 0.5 mM sodium pyruvate, 1× Insulin Transferrin Selenium (Roche Diagnostics, Mannheim, Germany), 100 nM dexamethasone (Sigma Aldrich), 0.17 mM L-ascorbic acid (Sigma Aldrich), 200 mM L-proline (Sigma Aldrich), 50 ng/mL Bone morphogenic protein 2 (BMP2, Peprotech, Rocky Hill, NJ, USA) and 0.5% methylcellulose (R&D Systems, Minneapolis, MN, USA). Immediately after seeding, the plates were centrifuged at 300 g for 10 min to accelerate spheroid formation. Plates were then transferred to the IncuCyte Zoom® system (IncuCyte-Sartorius, Ann Arbor, MI, USA), a live-cell imaging and

analysis platform, placed in a tri-gas incubator (Heracell V10S 250i, Thermo Fisher, Waltham, MA, USA) at 37 °C and 5% CO_2, to monitor spheroid formation. Spheroids were cultured for 7 days to allow ECM formation before treatment with NPs and irradiation.

Gadolinium Oxide Nanoparticles Treatment and Irradiation

GdoNP are composed of a polysiloxane shell surrounded by covalently bound 1,4,7,10-tetraazacyclododecane-1-glutaric anhydride–4,7,10-triacetic acid–Gd^{3+}. These nanoparticles are described by Sancey et al.[21]

In the 2-D culture, cells were seeded in 96-well plates at a density of 40,000 cells/cm^2 24 h before treatment with GdoNP. After washing, cells were incubated for 24 h at 37 °C with GdoNP suspended in the medium.

Spheroids cultured for 7 days in ULA round-bottom plates were incubated for 24 h at 37 °C with GdoNP suspended in the chondrogenic medium.

After 24 h incubation with the NPs, the 2-D and 3-D cultures were irradiated with a dose of 4 Gy delivered at once or fractionated (1 Gy during 4 consecutive days). X-ray irradiation was performed at a dose rate of 2 Gy/min using an X-Rad 320 irradiator (Precision X-ray Inc., North Branford, CT, USA) with an energy of 250 kV. Immediately after irradiation, the culture medium was carefully replaced with a fresh medium without GdoNP.

Cellular Uptake of GdoNP in Spheroids

HEMC-SS spheroids were treated with increasing concentrations of GdoNP and irradiated at 4 Gy. Seven days after treatment, the spheroids were dissociated by trypsinization, and cell viability was evaluated by the percentage of living cells (trypan blue exclusion).

Visualization of Fluorescent GdoNP Internalization in Cell Spheroids by Confocal Laser Scanning Microscopy

After 24 h incubation with 0.8 mM Cy5.5–GdoNP, spheroids were fixed with 4% paraformaldehyde (PFA, Santa Cruz Biotechnology, Dallas, TX, USA) and then incubated with 1 µg/mL of 4′,6-diamidino-2-phenylindole dihydrochloride (DAPI, Sigma Aldrich) for nuclear counterstaining. Ten-micrometre Z-stack images were acquired at 10× magnification using a Zeiss LSM 800 confocal laser scanning microscope from the CTµ platform (Centre Technologique des Microstructures, University Lyon 1, Villeurbanne, France) to visualize and localize internalized NPs.

Growth and Viability of 2-D and 3-D Cell Cultures

To monitor cell viability and growth, fluorescent cells were obtained by stable transduction with IncuCyte® NucLight-Lentivirus reagent (EFIα-Puro) (IncuCyte-Sartorius) that provides a homogeneous expression of a red fluorescent nuclear-restricted mKate2 protein. Briefly, 12 h before transduction, cells at 30% confluence were incubated in a serum-free medium supplemented with 8 µg/mL Polybrene infection reagent (Sigma Aldrich) and containing lentivirus at a multiplicity of infection (MOI = TU/cell) of 1.5. The transduction medium was then replaced with fresh medium and 48 h later, cells were selected with 1 µg/mL puromycin (Gibco) for 3 weeks. Cell transfection was stably maintained with 0.5 µg/mL puromycin.

After NPs and/or irradiation (4 Gy or 4 × 1 Gy) treatments, cells in the monolayer culture and spheroids in ULA plates were placed in the IncuCyte Zoom® imaging platform and the average fluorescence intensity (RFU) of mKate protein was measured in real time for each well. The Sensitizing Enhancement Ratio (SER_{4Gy}) was calculated as the ratio of the mean fluorescence intensity (% of control) calculated after 4 Gy irradiation and 4 Gy irradiation combined with GdoNP.

Immunofluorescence Staining of ACAN, Col2A1 in Spheroids

Seven days after treatment, spheroids were fixed for 30 min at room temperature in 4% PFA. After permeabilization and blocking, spheroids were incubated either with a mouse monoclonal ACAN antibody (#ab3778 Abcam, Cambridge, UK) or mouse monoclonal Col2A1 clone2B1.5 antibody (# MS-235-PO Thermo Fisher). A secondary Alexafluor 488-labelled

goat anti-mouse antibody was then used (#A11001 Invitrogen, Thermo Fisher Scientific). Cell nuclei were counterstained with DAPI. Images were captured using an Axio-Imager Z2 Zeiss fluorescence microscope (Carl Zeiss SAS, Le Pecq, France).

Cell Motility, Invasion and Migration

In 2-D-cultured cells, cell motility was assessed by the wound healing assay using the IncuCyte Zoom® device as described in Guy et al.[22]

In 3-D-cultured cells, cell migration from spheroids was measured in the IncuCyte Zoom® system after coating culture plates with Matrigel® for cell adherence. Briefly, after treatment, spheroids cultured in ULA round-bottomed plates were transferred into 125 µg/mL Matrigel®-coated (Corning Bedford, MA, USA) flat bottomed 96-well plates. Plates were then placed in the IncuCyte® and images were taken every 24 h until 96 h. The migration was measured as the area covered by the cells disseminating from the spheroid over the coated surface (ImageJ software, National Institutes of Health (NIH), MD, USA).

In 3-D-cultured cells, the invasion was measured in the IncuCyte® after spheroid embedding into 100 µL of 4.3 mg/mL Matrigel®. After Matrigel® polymerization for 1 h at 37 °C, 50 µL of chondrogenic medium were added to each well. Images were obtained every 24 h until 96 h and invasion was measured as the area covered by cells invading Matrigel® (ImageJ software).

Heterotopic HEMC-SS Tumor Model in Mice

All animals were treated according to the guidelines approved by the Ethics and Animal Welfare Committee of Claude Bernard Lyon 1 University (protocol numbers DR2015-30 and DR2017-50). After incubation for 10 days, HEMC-SS spheroids were harvested, rinsed and temporarily placed in PBS (Gibco) for transplantation. Six-week-old female NMRI nude mice (Janvier Labs, Saint Berthevin, France) were injected subcutaneously in the right flank with a suspension containing 30 HEMC-SS spheroids in 50 µL PBS and 50 µL of Matrigel™ (approximately 300000 cells in total). Body weight was monitored three times per week for each mouse as well as tumor growth. After eight weeks, tumors reached a size between 50 and 100 mm^3.

Radiolabelling of GdoNP

GdoNP (50 µL, 100 mM Gd) were radiolabelled by adding 300 µL of citrate buffer 50 mM pH 5 and 40–80 MBq of high purity $^{111}InCl_3$ (Mallinckrodt, Petten, Netherlands). The mixture was incubated for 30 min at 40 °C. Radiochemical purity (RCP) was evaluated using ITLC-SG (Tec-control black from Biodex Medical Systems, Shirley, NY, USA) and 50 mM citrate buffer (pH 5) as the mobile phase. The radiolabelled ^{111}In–GdoNP remained at the origin whereas the unbound $^{111}InCl_3$ migrated with a retention factor of 0.9–1. The ^{111}In–GdoNP stability was evaluated from 1 to 96 h by incubating the NPs at 37 °C in 2 mL of PBS supplemented with rat serum.

Biodistribution of GdoNP

Thirty-six nude mice bearing HEMC-SS heterotopic xenografts of approximately 150 mm^3 were used to evaluate the biodistribution of radiolabelled-GdoNP (IV and IT administrations). Eighteen mice received a 50 µL IT injection of ^{111}In–GdoNP (0.313 ± 0.079 MBq). Animals were sacrificed at 2 min, 10 min or 24 h (six animals per time after injection). Another group of 18 mice received a 100 µL IV injection of ^{111}In–GdoNP (0.748 ± 0.103 MBq). Animals were sacrificed at 10 min, 1 h or 24 h (six animals per time after injection).

The cadaver, brain, heart, liver, muscle, bone, skin, lung, spleen, kidney, knee, blood, gastrointestinal tract, tumor, gonads, urine and faeces of each sacrificed animal were harvested, weighed and conditioned in scintillation vials for counting. The radioactivity of each sample was measured using an automatic gamma scintillation counter (Wizard gamma counter, PerkinElmer, Waltham, MA, USA). The distribution of radiolabelled NPs was expressed as the percentage of injected dose per gram of tissue (% ID/g organ) and as the percentage of injected dose per organ (% ID/organ). The total injected dose was calculated by summing the activity of all organs, blood, cadaver, urine and faeces.

In vivo GdoNP Treatment and Irradiation

To evaluate the radiosensitizing effect of GdoNP, nude mice bearing heterotopic HEMC-SS xenografts of approximately 150 mm^3 were injected with vehicle alone (sodium chloride (NaCl) 9‰) or with a solution of GdoNP (IT or IV) diluted in the vehicle. Local irradiation was applied at an energy of 320 kV and a dose rate of 2 Gy/min using the X-Rad 320 irradiator. The experiments were divided into three sets. Before each set, mice were randomly selected for treatment and divided into different groups.

For the first set (n = 42), mice were divided into three groups: NaCl (n = 13), NaCl + 4 Gy (n = 12) and GdoNP + 4 Gy (n = 17). GdoNP was administrated intratumorally as a single injection of 50 µL (10 mM Gd). The irradiated groups received a single dose of 4 Gy 5 min after the injection of the vehicle or GdoNP.

For the second set (n = 72), mice were divided into five groups: NaCl (n = 6), GdoNP (n = 6), NaCl + 4 Gy 10 min post-injection (n = 20), GdoNP + 4 Gy 10 min post-injection (n = 20) and GdoNP + 4 Gy 24 h post-injection (n = 20). GdoNP was administrated IV as a single injection of 100 µL (100 mM Gd). The irradiated groups received a single dose of 4 Gy 10 min or 24 h after vehicle or GdoNP injection.

For the third set (n = 88), mice were divided into five groups: NaCl - IT (n = 9), NaCl - IT + 4 × 1 Gy (n = 20), GdoNP - IT + 4 × 1 Gy (n = 20), NaCl - IV + 4 × 1 Gy (n = 20), GdoNP - IV + 4 × 1 Gy (n = 19). The groups treated with GdoNP received 2 IT (10 mM Gd – 50 µL) injections or 2 IV (100 mM Gd – 100 µL) injections at 48 h intervals. The irradiated groups received 1 dose of 1 Gy each day for 4 days. The first radiation dose was delivered 2 min after the first injection.

All animals were monitored daily, the mouse weight and tumor size were measured twice a week. Tumor volume was calculated using the following formula: (width × $length^2$)/2, a percentage tumor growth curve and a survival curve were generated for each group. The animals were euthanized when the tumor reached 1000 mm^3. The studies were ended as soon as the last group reached the 50% survival mark.

Immunohistochemical Analysis of Tumors

TUNEL Analysis

TUNEL (terminal deoxynucleotidyl transferase dUTP nick end labelling) analysis was performed on 5 µm tissue sections to identify apoptotic cell death using a Dead End fluorometric TUNEL kit (Promega, Madison, WI, USA) according to the manufacturer's instructions. Digital images were obtained using a Zeiss Axio-Imager Z2 fluorescence microscope at 40× magnification. Apoptosis was quantified using ImageJ software. At least 150 nuclei per field were scored to calculate the average number of TUNEL-positive nuclei.

Immunodetection of PTX3

Paraffin sections were deparaffinized, rehydrated and antigen retrieval was performed in sodium citrate. The immunofluorescent staining protocol was identical to the one used for spheroids. Tumor slides were incubated with a polyclonal anti-PTX3 (#HPA069320 Atlas Antibodies Ozyme, St Quentin, France) and then with an Alexafluor 555-labelled donkey anti-rabbit (#ab150074 Abcam). Cell nuclei were counterstained with 1 µg/mL DAPI (Sigma Aldrich). Slides were visualized using a Zeiss Axio-Imager Z2 fluorescence microscope at 20× magnification.

Gene Expression Profile

Total RNA was isolated from 10 µm FFPE (Formalin-fixed –paraffin-embedded) - tumor sections with a High Pure FFPET RNA isolation kit (Roche Life Science, Germany (Cat #06650775001)) according to the manufacturer's instructions. RNA quantification and purity were assessed using a Nanodrop 2000 (Thermo Fisher Scientific). Isolated mRNAs (100 ng sample) were processed through the NanoString nCounter Prep Station (NanoString Technologies, Seattle, WA, USA) on the Hospices Civils de Lyon Platform. Gene expression profiles were established using the human nCounter PanCancer Progression Panel (NanoString Technologies) composed of 770 genes involved in angiogenesis, epithelial-to-mesenchymal transition (EMT), metastasis and ECM. Tumor samples were processed according to the manufacturer's instructions. Normalization of housekeeping genes for the quantification of gene expression levels, normalization of the positive control for background correction and data analysis were performed using the nSolver™

analysis software (NanoString Technologies). Transcripts with an RNA count < 20 for all samples were excluded because they were considered unexpressed. The mean and standard deviation (SD) were calculated for each group. Only genes with significant ($p < 0.05$) fold changes (< –2 or > +2) were considered as differentially expressed.

Statistical Analyses

For in vitro assays, results were expressed as the mean ± SD. Statistical significance was tested using two-way ANOVA or Student's *t*-test (GraphPad Prism 8.2, La Jolla, CA, USA) and was considered significant at $p < 0.05$ (* $p < 0.05$, ** $p < 0.01$, *** $p < 0.005$, **** $p < 0.001$).

For in vivo studies, results were expressed as mean ± SEM. The statistical significance of tumor growth curves was tested using Student's unpaired *t*-test and was considered significant at $p < 0.05$. Survival curves were compared using the non-parametric Log rank test and the Gehan–Breslow–Wilcoxon test (GraphPad Prism) and were considered significant at * $p < 0.0332$, ** $p < 0.0021$.

Results

In vitro Characterization of 2-D- and 3-D-Cultured HEMC-SS and SW1353 Chondrosarcoma Cell Lines

HEMC-SS and SW1353 cells presented a fibroblast-like phenotype in 2-D culture. SW1353 cells were clonogenic but not HEMC-SS ones.

Because 3-D cell cultures are more likely to mimic the natural tumor microenvironment, both cell lines were grown as spheroids in a chondrogenic culture medium. To facilitate efficient cell aggregation, methylcellulose, an inert adhesion-promoting matrix, was added to the culture medium. The HEMC-SS cell line formed loosely aggregated and irregular spheroids (Figure 1A i, ii) whereas SW1353 cells formed spherical and dense spheroids (Figure 1A v, vi). Seven days after seeding and formation, the spheroids were homogeneous in size, with high reproducibility, and the average diameter was 300–400 µm for HEMC-SS spheroids and 150–300 µm for SW1353 spheroids. The two ECM proteins, ACAN (Figure 1A iii, vii) and Col2A1 (Figure 1A iv, viii), were visualized using fluorescence microscopy after immunostaining in both HEMC-SS and SW1353 spheroids.

In the 2-D culture, the doubling time was 35 h for HEMC-SS cells and 20 h for SW1353 cells, whereas in the 3-D culture, the doubling time increased to 52 ± 1.2 h and 96 ± 1.2 h, respectively.

Optimization of Intracellular GdoNP Concentration

To determine the concentration of GdoNP that leads to the best radioenhancing effect, HEMC-SS spheroids were treated with an increasing concentration of GdoNP (100 to 1000 µM [Gd]) combined with 4 Gy irradiation. The dose–response curve (Figure 1B) indicated a concentration of 800 µM [Gd] as the best compromise between radiosensitization and the absence of cytotoxicity up to 7 days of treatment (data not shown). The same concentration was also selected for SW1353 spheroids.

Uptake and Localization of GdoNP in Spheroids

To control whether the NPs were entering the cells, the uptake of 800 µM Cy5-5 labelled GdoNP was visualized using confocal microscopy after 24 h of incubation with both types of spheroids (Figure 1C and D). The 10-µm Z-stacking allowed visualization of GdoNP from the edge of the spheroid to a depth of 70 µm. Internalized NPs were observed from 40 µm to 70 µm for HEMC-SS (Figure 1C v–viii) with comparable intensity, whereas in SW1353 spheroids, they were observed from 30 µm (Figure 1D iii) to the centre of the spheroid (Figure 1D viii) with maximum intensity at 40 µm (Figure 1D iv).

GdoNP Sensitizes HEMC-SS and SW1353 Cells to Photon Radiation

For both NucLight-red-transduced cell lines, the fluorescence of the mKate2 nuclear protein allowed tracking and quantification of living cells. Because classical clonogenic survival curves were not feasible for HEMC-SS cells, the response to irradiation, combined or not with GdoNP, was assessed by monitoring the total fluorescence intensity of the transduced cells. In Figure 2A and B, the radiosensitizing effect was expressed as the mean fluorescence intensity after

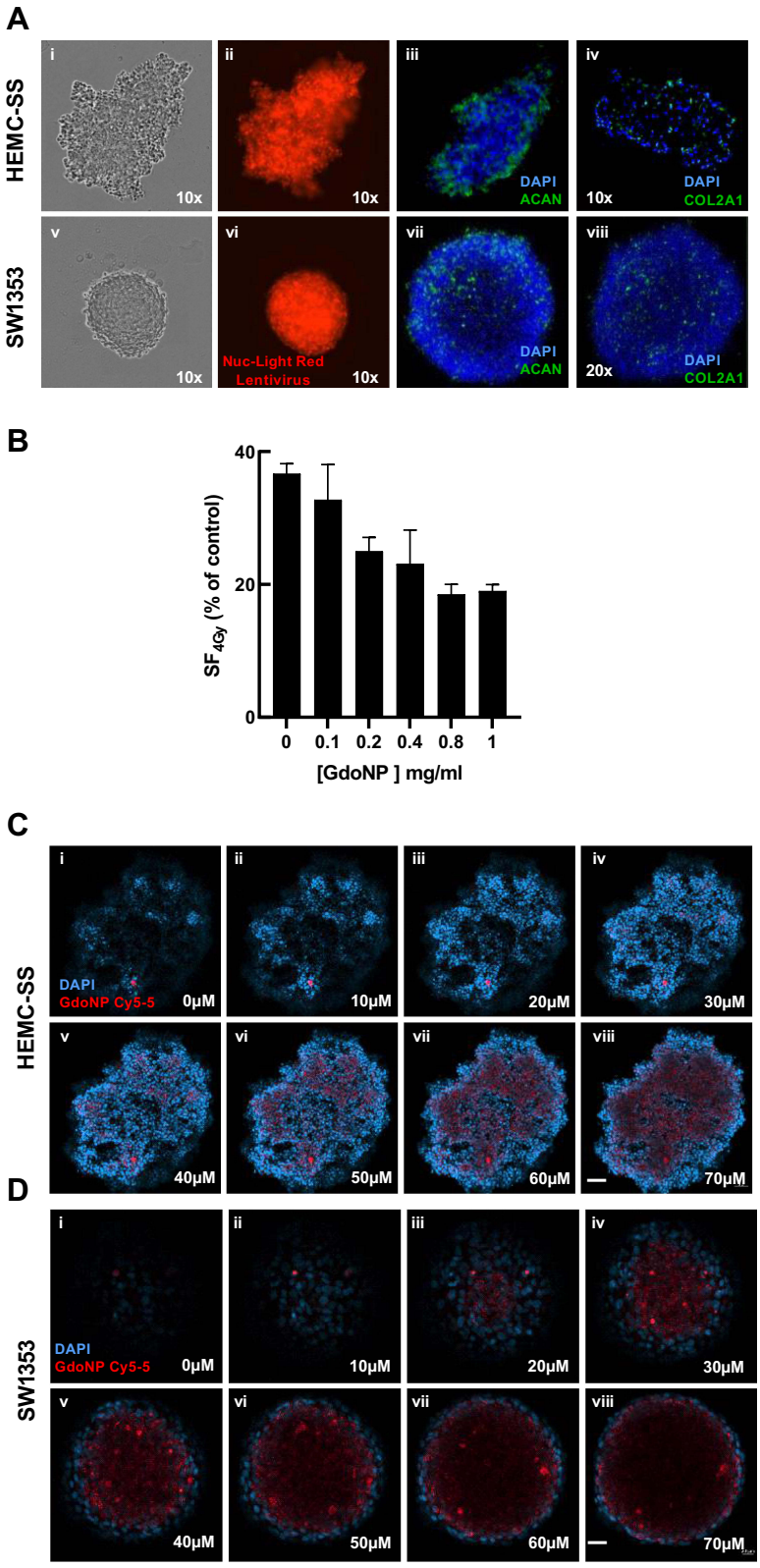

Figure 1 Characterization of CHS spheroids and cellular uptake of GdoNP. (**A**) Phase contrast (i, v) and fluorescent (ii, vi) images of HEMC-SS and SW1353 spheroids stably expressing NucLight-Red Lentivirus; immunofluorescent staining of ACAN (iii, vii) or Col2A1 (iv, viii) (green) and of nuclei with DAPI (blue). (**B**) The surviving fraction at 4 Gy versus 0 Gy of 7 days HEMC-SS spheroids after 24 h incubation with different GdoNP concentrations. (**C**) Confocal microscopy images, every 10 μm sections of a HEMC-SS cell spheroid (i, ii, iv, v, vi, vii, viii), realized 24 h after the addition of 800 μM GdoNP conjugated to Cy5-5 (**D**) idem as (**C**) with SW1353 spheroids (Scale bar HEMC-SS: 50 μm, scale bar SW1353: 20 μm).

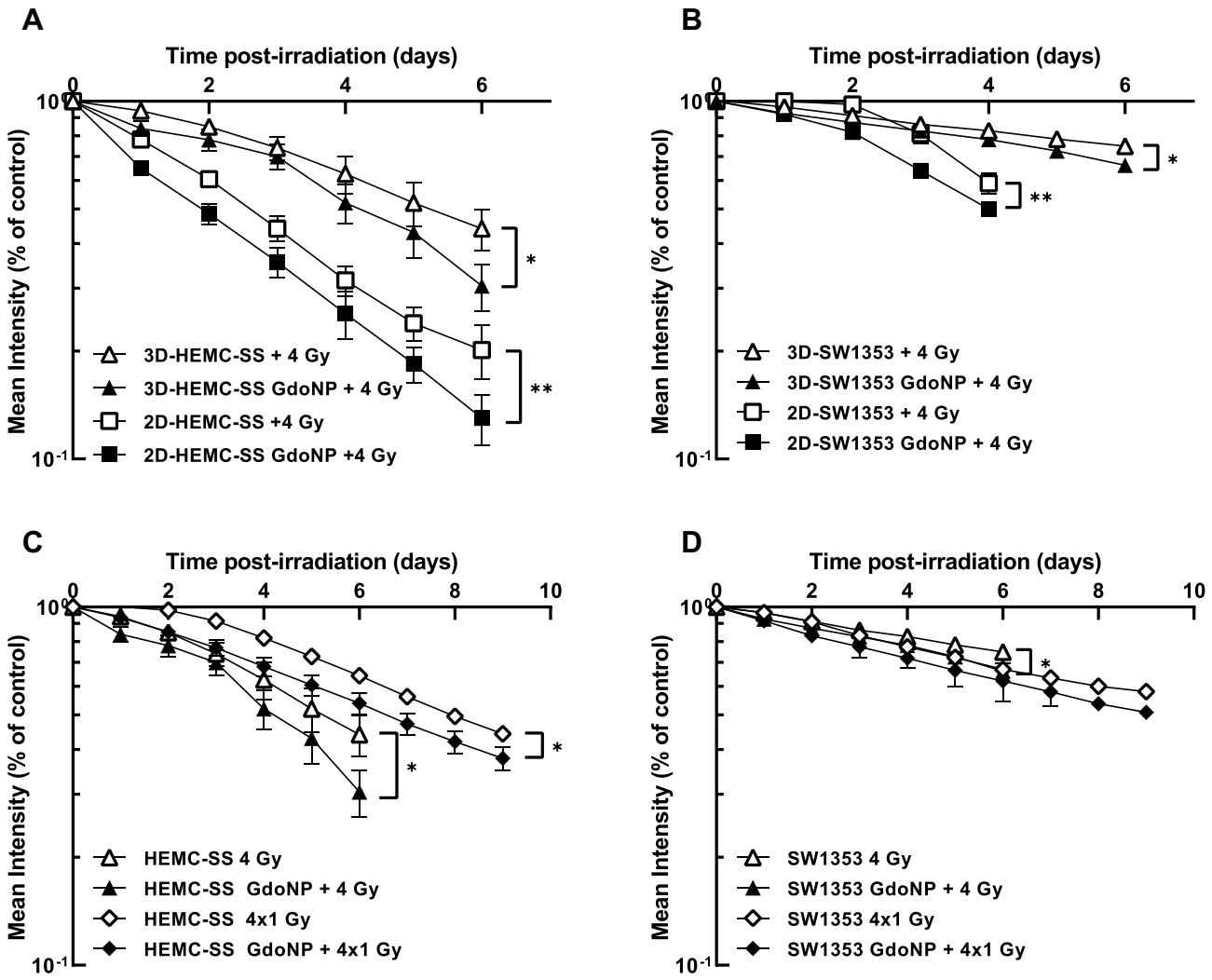

Figure 2 Radiosensitizing effect of GdoNP combined with 4 Gy irradiation in 2-D and 3-D CHS cells. Kinetics of mKate2-expression by HEMC-SS cells (**A**) or SW1353 cells (**B**), cultured in 2-D and 3-D, in response to 4 Gy irradiation combined or not with GdoNP. Kinetics of mKate2-expression by HEMC-SS spheroids (**C**) or SW1353 spheroids (**D**), in response to a single 4 Gy or 4×1 Gy fractionated irradiation combined or not with GdoNP. Results are expressed as the mean fluorescence intensity of transduced irradiated cells relative to non-irradiated cells. Each value represents the mean ± SD of two independent experiments performed in 12 replicates (*$p < 0.05$, **$p < 0.01$).

4 Gy irradiation, associated or not with GdoNP, relative to non-irradiated cells. Cells grown as spheroids were more resistant to irradiation than in a 2-D culture, especially in SW1353 cells which were more resistant than HEMC-SS cells. Six days after 4 Gy irradiation, the means of fluorescence, in 2-D and 3-D cultures were 0.2 ± 0.03 and 0.44 ± 0.06, respectively, for HEMC-SS cells and 0.59 ± 0.02 and 0.75 ± 0.02 for SW1353 cells. When the cells were incubated for 24 h with GdoNP (800 µM [Gd]), before irradiation, the means of fluorescence in 2-D and 3-D cultures significantly decreased to 0.13 ± 0.02 and 0.30 ± 0.05 for HEMC-SS cells, respectively, and 0.50 ± 0.02 and 0.66 ± 0.03 for SW1353 cells. For each cell line, 6 days after irradiation, the Sensitizing Enhancement Ratio (SER_{4Gy}) of GdoNP treatment was roughly the same for 2-D and 3-D cultures, but higher for HEMC-SS (1.4) than for SW1353 (1.1).

To get even closer to the conditions used in the clinic, the effect of GdoNP combined with a fractionated irradiation was also studied. Thus, after a 24 h treatment with GdoNP, the spheroids were irradiated with 1 Gy for 4 consecutive days (Figure 2C and D). As expected, fractionated irradiation led to a higher survival than with a single irradiation of 4 Gy. Nine days after the first irradiation of 1 Gy, the combination of GdoNP with fractionated irradiation resulted in a $SER_{4\times1Gy}$ of 1.2 for HEMC-SS and 1.1 for SW1353 cells. Overall, these results demonstrate that GdoNP sensitizes CHS cells to irradiation.

In vivo Distribution of ^{111}In–GdoNP in the HEMC-SS Model

First, the stability of radiolabelled ^{111}In–GdoNP was evaluated to assess its future in vivo tolerance. After incubation in PBS (pH 7.4) supplemented with rat serum for 96 h, the RCP was greater than 96%, indicating that this complex was stable and therefore suitable for in vivo experiments.

Next, to evaluate the different biodistribution profiles after two types of administration (IT and IV), the amount of ^{111}In–GdoNP in HEMC-SS tumor-bearing mice was determined with scintigraphy at the following time points: 2 min, 10 min and 24 h after one IT injection and 10 min, 1 h and 24 h following one IV injection (Supplementary Data Tables S1 and S2).

A maximal dose of ^{111}In–GdoNP was measured at 2 and 10 min post-IT administration and high levels remained in the tumor at 24 h (79.1 ± 17.5% of ID/g of tumor) (Figure 3). Increasing levels of ^{111}In–GdoNP in the kidneys were observed over time, indicating good renal elimination.

After IV injection, ^{111}In–GdoNP was found in the kidneys from 10 min to 24 h, with a peak at 1 h (94.7 ± 9.8% ID/g of organ and 131.5 ± 9.6% ID/g of organ, respectively). EPR-mediated accumulation of AGuIX in the tumors increased with time (1.1 ± 0.2 and 2.2 ± 0.5% ID/g of tumor, respectively, at 10 min and 24 h after injection).

Importantly, for both types of administration, no significant retention of radiolabelled NPs in other organs, including the brain and liver, was observed (Supplementary Data Tables S1 and S2, Figure 3). In addition, faecal excretion was low, demonstrating that the NPs do not interfere with the gastrointestinal tract.

In vivo Radiosensitizing Effect of GdoNP

To find the best combination to overcome CHS radioresistance, the efficacy of GdoNP as a radiosensitizing agent was evaluated under four conditions: irradiation with a single dose of 4 Gy or with a fractionated dose of 4 Gy (1 Gy per day for 4 days) after IT or IV administration of GdoNP.

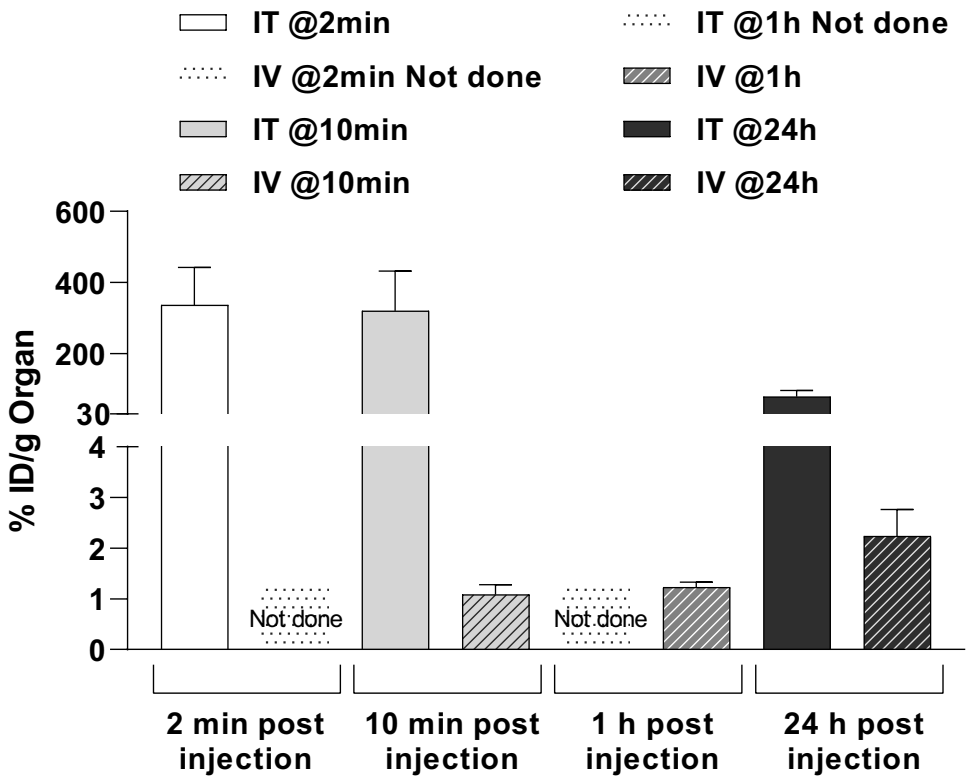

Figure 3 In vivo distribution of ^{111}In–GdoNP in the HEMC-SS model. Percentage of injected dose per gram of tumor at several times after an IT or an IV injection of ^{111}In–GdoNP in NMRI nude mice bearing HEMC-SS xenograft (mean ± SEM).

Combination of GdoNP (IT or IV) with a Single Dose of X-Ray (4 Gy)

IT Administration of GdoNP

A single-dose irradiation of 4 Gy 5 min after an IT injection of GdoNP resulted in a significant decrease in tumor growth compared with irradiation alone (* $p < 0.05$, Figure 4A). This reduction of tumor growth was associated with a significant increase (* $p < 0.05$) in the median survival of mice that received the combined treatment (87 days) compared with mice that received only irradiation (56 days) (Figure 4C).

To investigate further the effect of the combination of GdoNP (IT administration) and irradiation (4 Gy), apoptotic cell death was quantified by TUNEL staining (Figure 4E). As expected, irradiation alone resulted in a small increase in apoptotic cells compared with the untreated group whereas the addition of GdoNP significantly increased it (*** $p <$ 0.005 compared with the irradiated group, Figure 4F).

IV Administration of GdoNP

As shown in the biodistribution study, IV injection of GdoNP led to an increased tumor uptake during the first 24 h. Therefore, to determine the best therapeutic strategy to achieve the optimal radiosensitization, the mice were irradiated for 10 min or 24 h after GdoNP injection. IV administration of GdoNP alone did not exert any significant anti-tumor effect on tumor-bearing mice, either on tumor growth or survival (Figure 4B–D). Tumor growth in mice irradiated 10 min after GdoNP injection was significantly lower than in mice only irradiated (* $p < 0.05$). It is interesting to note that irradiating 24 h after the injection of GdoNP reduces tumor growth more than irradiating 10 min after injection (* $p < 0.05$).

In contrast to IT administration, IV injection of GdoNP did not significantly prolong the median survival of mice compared with irradiated mice (Figure 4D).

Combination of GdoNP (IT or IV) with a Fractionated Dose of X-Rays (4 × 1 Gy)

To get one step closer to the clinic, the efficacy of GdoNP combined with fractionated irradiation has been evaluated. HEMC-SS tumor-bearing mice were irradiated at 1 Gy for four consecutive days. The mice concerned received two injections (IT or IV) of GdoNP or NaCl before the 1st and 3rd irradiations.

In association with irradiation, GdoNP significantly decreased tumor growth compared with the irradiated groups, regardless of the mode of administration (*** $p < 0.005$, Figure 5A and B). Interestingly, unlike in the control group and irradiated groups, tumor relapse was observed in mice treated with GdoNP (IT and IV) and irradiation, the week following the end of treatment (Figure 5C). However, the tumors started to grow again and returned to their initial size 11 or 13 days after the beginning of the treatment. GdoNP combined with fractionated irradiation significantly increased the median survival of mice only when injected by IT (* $p < 0.05$, Figure 5D). Although IV injection of GdoNP altered tumor growth, it did not significantly prolong mice survival (Figure 5E).

Differential Expression of PTX3 in Mice Treated with GdoNP (IV Injection) Combined with Irradiation

To identify the pathways that led to tumor regression in mice treated with GdoNP during the first days following the fractionated irradiation, RNA was extracted from three tumors of each group of mice euthanized 7 days after treatment and the gene expression profile was quantified with the "human nCounter PanCancer Progression" panel (770 genes) on a NanoString® platform. Four genes, C-X-C Chemokine Receptor 4 (CXCR4), Myosin 5C (MYO5C), Plastin 1 (PLS1) and Pentaxin 3 (PTX3), were identified as differentially expressed between the irradiated+IV-GdoNP and 4×1 Gy irradiated groups of mice. PTX3 and CXCR4 activate the EMT, which participates in the metastatic process, whereas MYO5C and PLS1 activate the reverse process named mesenchymal-to-epithelial transition (MET). Their normalized numbers of transcripts are shown in Figure 6A. Even if it is not statistically significant, the irradiation treatment increased PTX3, the RNA count being 1.9 times higher than in the control group. In response to the combined treatment, PTX3 expression was strongly decreased (fold change: 3.7) compared with irradiation alone (** $p < 0.01$). Conversely, irradiation decreased CXCR4, MYO5C, and PLS1 numbers of transcripts (*ns*) and increased them after combined treatment (* $p<0.05$, *** $p < 0.001$). Because the expression of these three genes was low in the three groups of mice

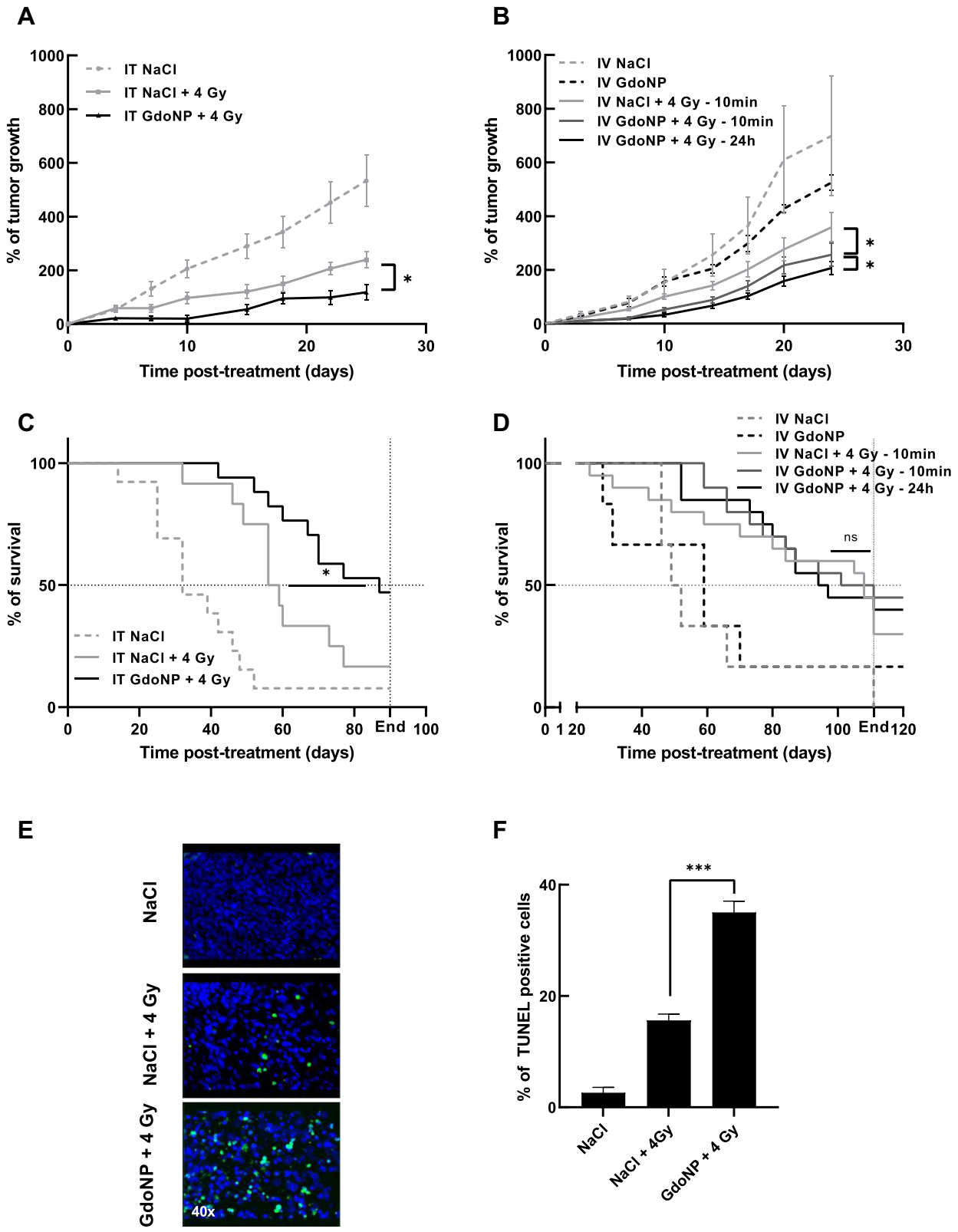

Figure 4 In vivo radiosensitizing effect of GdoNP, after IT or IV injection, combined with a single 4 Gy irradiation. Evolution of tumor growth (**A**) after IT or (**B**) after IV injection, expressed as mean% of tumor growth ± SEM. Survival curve (**C**) after IT injection or (**D**) after IV injection. (**E**) Detection of apoptosis using TUNEL staining on paraffin-embedded tumor sections after animal sacrifice at the limited volume of 1000 mm^3 (40× magnification). (**F**) Percentage of apoptotic cells in each group of treatment. Each value represents the mean number ± SEM of TUNEL-positive cells in three random fields per slide assessed in triplicate. (*$p < 0.05$, ***$p < 0.005$).
Abbreviation: ns, non significant.

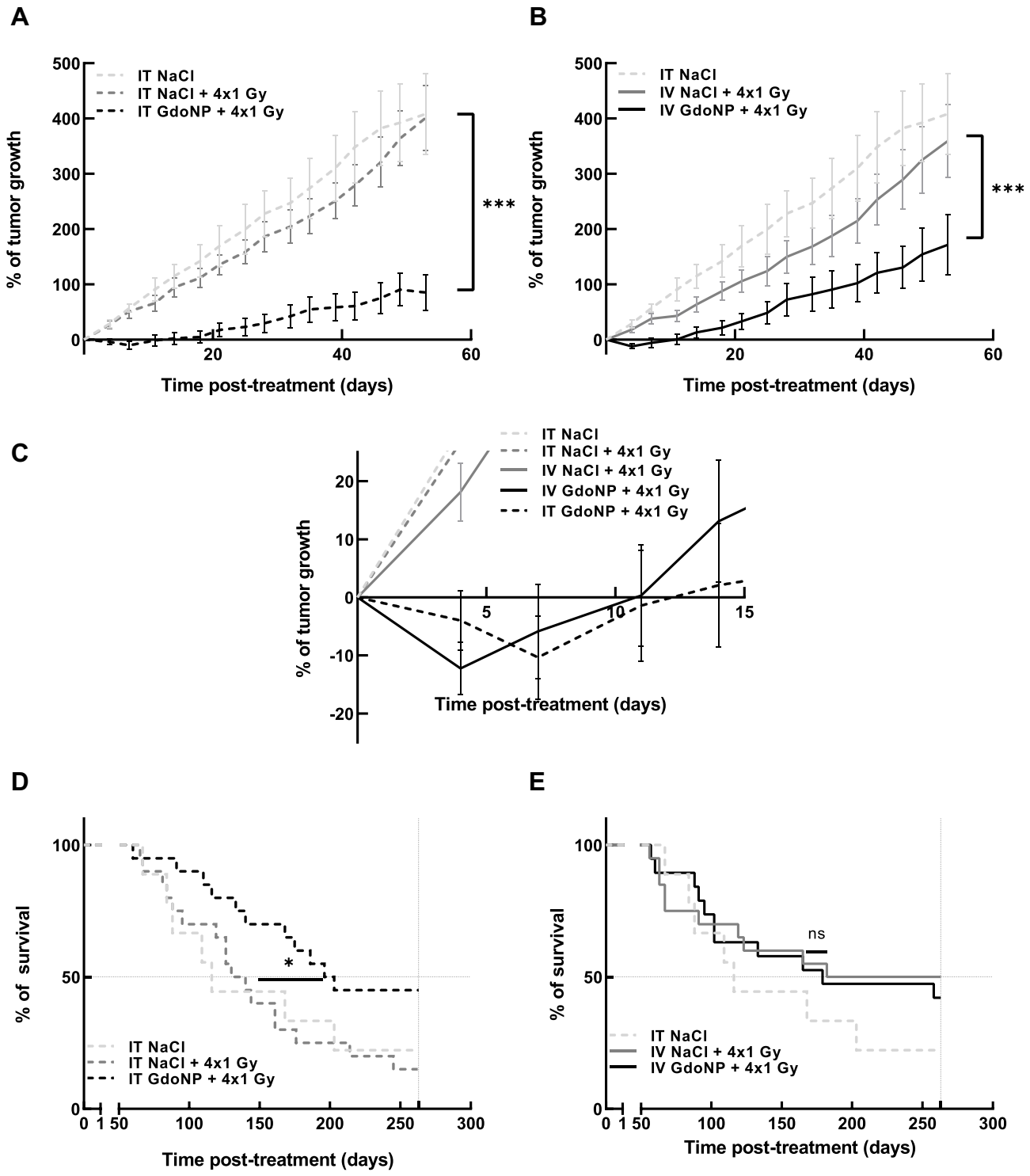

Figure 5 In vivo radiosensitizing effect of GdoNP, after IT or IV injection, combined with a 4×1 Gy fractionated irradiation. (**A**) Evolution of tumor growth after IT injection of GdoNP combined or not with irradiation, expressed as mean% of tumor growth ± SEM. (**B**) Evolution of tumor growth after IV injection of GdoNP combined or not with irradiation, expressed as mean% of tumor growth ± SEM. (**C**) Zoom of graphs A and B to display the evolution of tumor growth within the first 15 days after treatment. (**D**) Survival curves after IT injection combined with fractionated irradiation. (**E**) Survival curves after IV injection combined with fractionated irradiation. (*$p < 0.0332$; ***$p < 0.005$).

Abbreviation: ns, non significant.

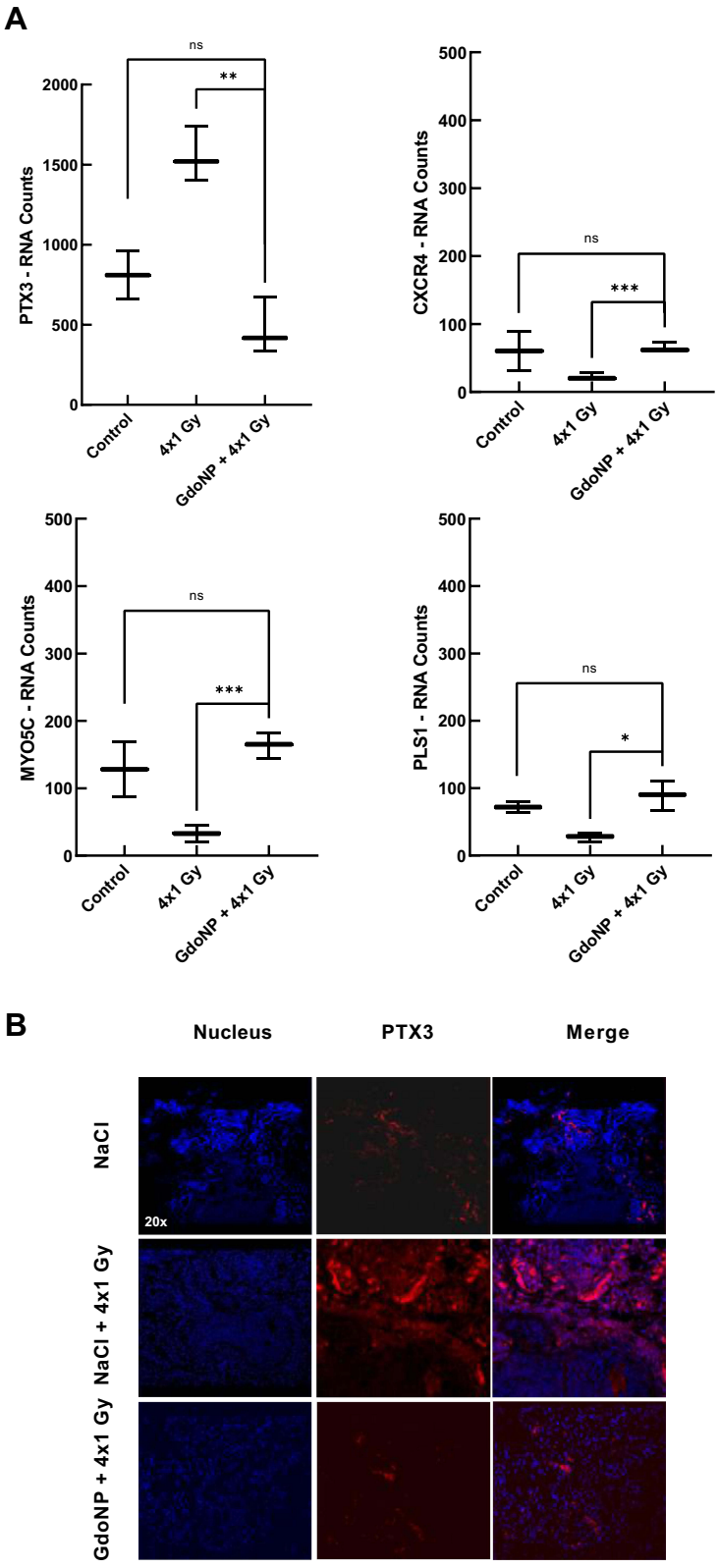

Figure 6 Gene expression of PTX3, CXCR4, MYO5C or PLS1 and PTX3 protein expression in tumors of mice sacrificed 7 days after treatment. (**A**) Box plots of RNA expression counts (median ± 1.5 times the interquartile range) for PTX3, CXCR4, MYO5C or PLS1 genes in three tumors of each group of treatment (NaCl, NaCl + 4×1 Gy and GdoNP (IV) + 4×1 Gy). (**B**) Fluorescent immunostaining of PTX3 protein (red) and nuclei (DAPI) in tumor sections for one mouse from each group of treatments. (*p < 0.05, **p<0.01, ***p<0.005).

Abbreviation: ns, non significant.

(RNA counts less than 150), only the PTX3 protein expression was studied using IHC (Immunohistochemistry) to confirm the results. As expected, a very high expression of PTX3 protein was observed in the tumor section of mice treated with GdoNP and irradiation compared with the absence of expression in the control and irradiated groups (Figure 6B).

GdoNP Decreases the Migratory and Invasive Capacities of CHS Cells

To confirm the in vivo results concerning gene expression variations related to EMT, experiments were then conducted in 2-D and 3-D HEMC-SS and SW1353 cell culture to evaluate the effect of GdoNP, combined or not with irradiation, on the migration and invasion processes. Motility was first quantified by the classical wound healing assay in 2-D cultures. Only 11% ± 1% of the wound was sutured after 48 h for HEMC-SS control cells (Figure 7A) whereas the suturing reached 84.8% ± 8.2% for SW1353 cells (Figure 7A and B). At 48 h, for both cell lines, the addition of GdoNP or 4 Gy irradiation alone did not significantly alter cell motility whereas the combination of GdoNP with irradiation significantly decreased motility compared with control cells (**** $p < 0.001$) or with irradiated cells (** $p < 0.01$ for HEMC-SS cells and **** $p < 0.001$ for SW1353 cells).

For the 3-D migration assay, the area occupied by cells disseminated from the spheroids was recorded every 24 h up to 96 h and analysed using ImageJ software (Figure 7C and D). GdoNP treatment alone did not influence the migration. Irradiation alone increased 3-D cell migration for SW1353 cells only. At 96 hour, the combination of GdoNP and irradiation significantly decreased migration, resulting in a 45.9% ± 6.1% decrease in migration compared with irradiated spheroids for HEMC-SS (**** $p < 0.001$) and 20.8% ± 3.1% for SW1353 (**** $p < 0.001$).

To measure tumor spheroid invasion, Matrigel® was added to the wells immediately after irradiation to provide a semi-solid gel-like matrix. The HEMC-SS spheroids consisted of a very compact core area surrounded by a less dense area containing invasive cells with weak interactions. The SW1353 invasive cells were distributed in an array around the spheroid. The area of the less dense zone was used to measure cell invasion (Figure 7E and F). Cell treatment with GdoNP alone did not influence the invasion process. Irradiation alone led to fluctuating responses depending on the time point and cell line but rarely significantly. Finally, at 96 h, the combination of GdoNP with irradiation significantly decreased cell invasion compared with control spheroids (54.3% ± 5.4% (**** $p < 0.001$) for HEMC-SS and 44.8% ± 2.1% for SW1353 (*** $p < 0.001$) and also compared with irradiation alone (**** $p < 0.001$)).

Discussion

Because CHSs show a heterogeneous response to photon irradiation,[23] the radiosensitizing effect of GdoNP was investigated in this work, first in vitro, in two subtypes of CHS cell lines, and then in vivo in a tumor-implanted murine model of CHS. As expected, the interactions of GdoNP with photons increased the killing effect of irradiation in CHS cells. In vivo, a single or a fractionated dose of 4 Gy associated with IT or IV injection of GdoNP significantly decreased tumor growth. In the experimental conditions tested, only IT injection increased mice survival. Unexpectedly, the radiosensitizing effect was associated in vitro with a significant decrease in cell migration and invasion and in vivo with the decreased expression of PTX3 which is involved in the EMT process, highly suggesting a potential impact of GdoNP on metastasis formation.

Cancer therapies are frequently tested in 2-D cell culture models. Most treatments found promising on cell cultures have little or no efficacy in patients because the 2-D culture systems lack the structural architecture and microenvironment of the tumor.[24] In spheroids, an important role is played not only by cell–cell interactions but also by internal or external biochemical signals that are part of the tumor microenvironment. Indeed, CHS spheroid models have been set up to maintain the natural morphology of chondrocytes and produce a cartilaginous matrix resembling the original tumor biopsy.[25] It is thus a more reliable in vitro model for this pathology, especially to study the radio- or chemoresistance of CHS[26] and to evaluate the efficacy of drugs.[24,27,28]

In this study, the radiosensitization potential of GdoNP was first demonstrated in vitro, in 2-D and 3-D cultures of a soft sarcoma (HEMC-SS cell line) and a conventional CHS (SW1353 cell line) after a single dose or a fractionated irradiation (1 Gy/day for 4 days). They confirm the data obtained with GdoNP in other radioresistant tumor cell models

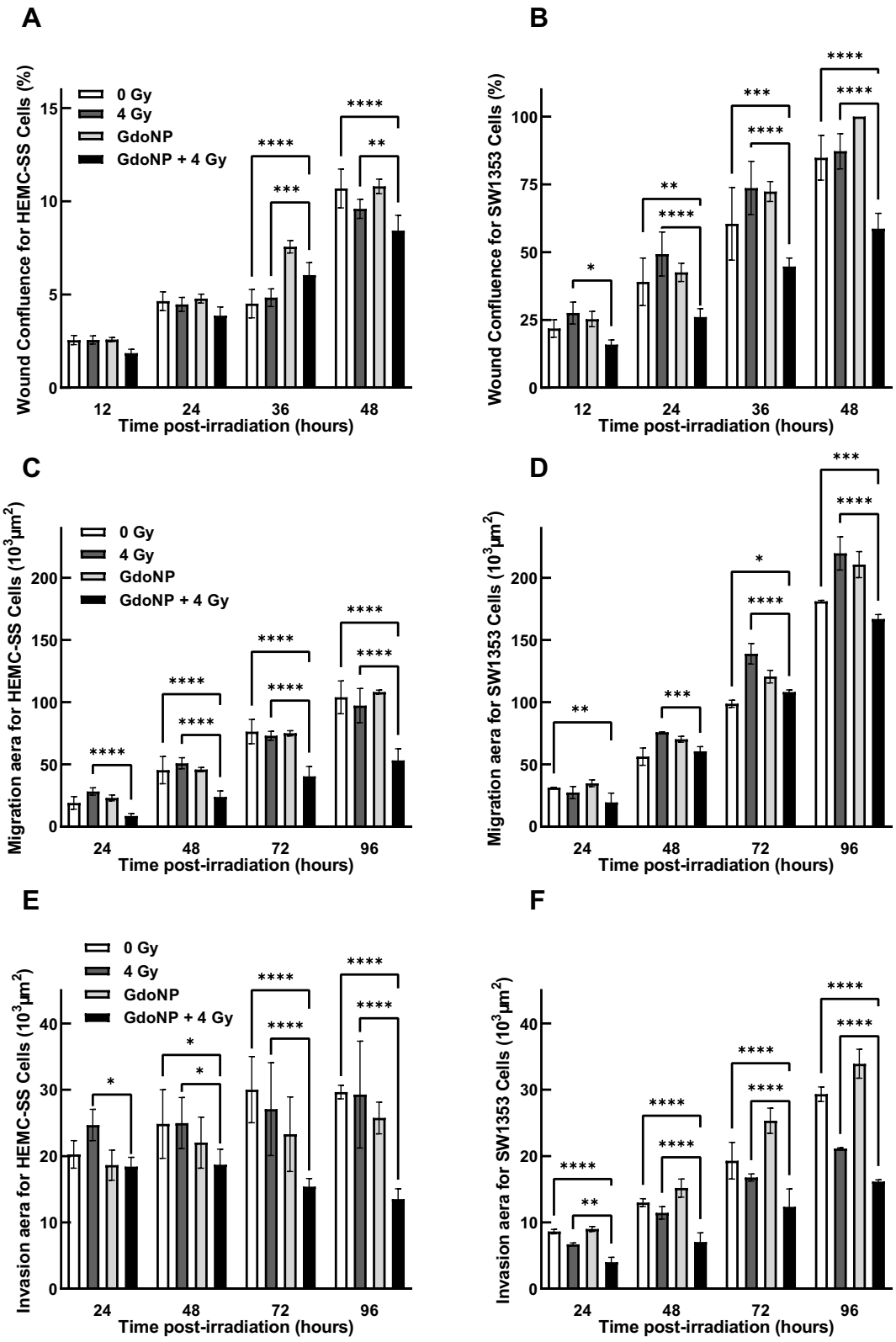

Figure 7 Impact of GdoNP treatment combined or not with irradiation on the CHS cell migration and invasion processes. Quantification of cell motility in 2-D HEMC-SS (**A**) and SW1353 (**B**) cells irradiated at 4 Gy in the presence or not of 800 µmol GdoNP. Quantification of cell migration in HEMC-SS (**C**) or SW1353 (**D**), spheroids and cell invasion in HEMC-SS (**E**) and SW1353 (**F**) spheroids treated in the same conditions. Each value represents the mean ± SD of two independent experiments performed in 12 replicates (*$p < 0.05$, **$p < 0.01$, ***$p < 0.005$, ****$p<0.001$).

such as HNSCC,[29–31] glioblastomas[32] or brain melanoma metastasis.[19] A concentration of 800 μM [Gd] was selected for in vitro experiments, similar to that used in our previous works.[30,31,33]

CHSs are tumors known to be radio- and chemoresistant, and finding effective therapeutic strategies is a challenge. Because CHSs constitute a heterogeneous group of primary bone cancers, multiple oncogenic pathways have been implicated in these mechanisms[7,26] and numerous studies have sought to understand the mechanisms involved in their resistance to apoptosis.[24,34,35] Alterations of cell cycle due to mutations of isocitrate dehydrogenases (IDH1 and IDH2),[1,36,37] activation of the mTOR/AkT pathways[38] and EMT process[28,39] have also been involved in their resistance to treatments. The hypoxic conditions inherent in the microenvironment of CHS tumors could also partly explain their radioresistance because the production of ROS induced by radiation will be lower.[40]

In vivo, radiosensitization was demonstrated with an increase in the mean survival of mice following radiation exposure only after IT injection of GdoNP. After IV injection and fractionated irradiation, tumor regression was observed only in the first days after irradiation. Because tumors were poorly vascularized in heterotopic xenografts, the passive accumulation of GdoNP by the EPR effect was certainly lower. As a consequence, ionization of NPs by photons produced only a small number of secondary particles (photoelectrons, Auger, Compton electrons etc.) that resulted in a radiosensitizing effect too weak to decrease tumor growth over a long period. These results suggest that an optimal treatment scheme will require several injections of GdoNP during the radiotherapy protocol to improve the radiosensitization effect.

The analysis of RNA transcripts using nCounter NanoString® identified four genes differentially expressed in tumors of animals sacrificed after receiving the combination treatment, PTX3, CXCR4, MYO5 and PLS1, which are all involved in the metastatic process. Because CXCL12, the ligand of CXCR4 is not expressed, CXCR4 will not be able to activate angiogenesis and metastasis formation.[41] On the other hand, the increased expression of MYO5C and PLS1 could activate the MET, the reverse process of the EMT.[42] Finally, the expression of PTX3, a gene involved in EMT,[42] is the one that is most significantly impacted in response to the combined treatment. Its decrease was confirmed by the IHC staining of PTX3 protein in the same tumor sections. PTX3 decrease could be correlated with the inhibition of EMT as previously described in different types of cancer cell lines (breast cancer cells,[43] human cervical cancer cells[44] and glioma cells)[45] as well as in biopsies of bone metastatic breast cancer[46] and hepatocellular carcinoma.[47] To validate these preclinical results, we returned to the cellular model and confirmed the significant decrease in cell invasion and migration in HEMC-SS spheroids treated with the combination of GdoNP and irradiation. This unexpected effect of GdoNP on the invasion and migration of cultured cells and on PTX3 over-expression in tumor sections is of great importance because metastasis formation is a major obstacle to the successful treatment of CHSs.

Based on promising preclinical results of GdoNP on more than 12 animal models showing high radiosensitization properties,[17] a Phase 1 clinical trial was conducted (NCT02820454) in 15 patients with multiple brain metastases.[19,20] A single IV administration of GdoNP was performed and patients received whole-brain radiotherapy. No AGuIX-related adverse effects have been observed and NPs were shown to accumulate and be retained in all types of brain metastases. First insights of radiosensitization have been shown on 13 patients, and four Phase 2 or Phase 1/2 clinical trials have begun on different indications in Europe and the US. Besides, another radiosensitizing NP, containing hafnium atoms, named NBTXR3, was developed and brought to the clinic by Nanobiotix. A Phase 2/3 randomized controlled trial in patients with locally advanced soft tissue sarcoma of the extremities or trunk wall is ongoing after IT injection of these particles.[48] GdoNP has a great advantage over NBTXR3 because it is a positive contrast agent for magnetic resonance imaging. It can thus be used to delimit tumors precisely before combining it with radiotherapy.

Finally, we validated in preclinical models the therapeutic potential of the hybrid theranostic GdoNP upon radiation exposure in CHS. This proof of concept provided strong arguments to launch an interregional Clinical Research Hospital Programme (PHRC) in 2021. NANO-RT-MSK is a multicentre, randomized Phase 2 trial evaluating the association of GdoNP with radiotherapy for the therapeutic management of patients with symptomatic inoperable musculoskeletal tumor lesions.

Abbreviations

ACAN, Aggregan; AGuIX, Activation and Guidance of Irradiation by X-ray; CHS, chondrosarcoma; Col2A1, Collagen type 2 α1; CXCL12, Stromal cell-derived factor; CXCR4, CXC-Motif Chemokine Receptor 4; ECM, Extra-cellular matrix; EM-CHS, Extra-skeletal myxoid chondrosarcoma; EMT, Epithelial-to-mesenchymal transition; EPR, Enhanced permeability and retention; FFPE, Formalin-fixed –paraffin-embedded; ID, Injected dose; IHC, Immunohistochemistry; IT, Intratumoral; IV, Intravenous; MET, Mesenchymal-to-Epithelial Transition; MYO5C, Myosin 5C; NPs, Nanoparticles; PLS1, Plastin 1;PTX3, Pentraxin 3; RCP, radiochemical purity; ROS, Reactive oxygen species; RT, high-dose radiation therapy; TUNEL, Terminal deoxynucleotidyl transferase dUTP nick end labelling.

Acknowledgments

This work was funded and supported by the CHONDRAD ANR program (ANR14CE 16-0021) and LABEX PRIMES (ANR-11-LABX-0063) of Université de Lyon, within the programme 'Investissements d'Avenir' (ANR-11-IDEX-0007) operated by the French National Research Agency (ANR). We would like to thank Emma Armandy (UMR CNRS5822/IP2I) for her technical assistance and Dr Gersende Alphonse (UMR CNRS5822/IP2I, HCL) for her help in editing the figures and proofreading the manuscript.

Author Contributions

All authors made a significant contribution to the work reported, whether that is in the conception, study design, execution, acquisition of data, analysis and interpretation, or in all these areas; took part in drafting, revising or critically reviewing the article; gave final approval of the version to be published; have agreed on the journal to which the article has been submitted; and agree to be accountable for all aspects of the work.

Supplementary Material

Supplementary Table S1 and S2.

Disclosure

F.L. and O.T. have one patent (WO2011135101) protecting the GdoNP, are employed by NH TherAguix owner of AGuIX® and possess shares in this company. The authors report no other conflicts of interest in this work.

References

1. de Jong Y, Ingola M, Briaire-de Bruijn IH, et al. Radiotherapy resistance in chondrosarcoma cells; a possible correlation with alterations in cell cycle related genes. *Clin Sarcoma Res*. 2019;9(1):9. doi:10.1186/s13569-019-0119-0
2. Davis EJ, Wu YM, Robinson D, et al. Next generation sequencing of extraskeletal myxoid chondrosarcoma. *Oncotarget*. 2017;8(13):21770–21777. doi:10.18632/oncotarget.15568
3. Paoluzzi L, Ghesani M. Extraskeletal myxoid chondrosarcoma with massive pulmonary metastases. *Clin Sarcoma Res*. 2018;8(1):20. doi:10.1186/s13569-018-0108-8
4. Willems SM, Schrage YM, Baelde JJ, et al. Myxoid tumours of soft tissue: the so-called myxoid extracellular matrix is heterogeneous in composition. *Histopathology*. 2008;52(4):465–474. doi:10.1111/j.1365-2559.2008.02967.x
5. Mery B, Espenel S, Guy JB, et al. Biological aspects of chondrosarcoma: leaps and hurdles. *Crit Rev Oncol Hematol*. 2018;126:32–36. doi:10.1016/j.critrevonc.2018.03.009
6. Muz B, de la Puente P, Azab F, Azab AK. The role of hypoxia in cancer progression, angiogenesis, metastasis, and resistance to therapy. *Hypoxia*. 2015;3:83–92. doi:10.2147/HP.S93413
7. Speetjens FM, de Jong Y, Gelderblom H, Bovée JV. Molecular oncogenesis of chondrosarcoma: impact for targeted treatment. *Curr Opin Oncol*. 2016;28(4):314–322. doi:10.1097/CCO.0000000000000300
8. Gelderblom H, Hogendoorn PCW, Dijkstra SD, et al. The clinical approach towards chondrosarcoma. *Oncologist*. 2008;13(3):320–329. doi:10.1634/theoncologist.2007-0237
9. Polychronidou G, Karavasilis V, Pollack SM, Huang PH, Lee A, Jones RL. Novel therapeutic approaches in chondrosarcoma. *Future Oncol*. 2017;13(7):637–648. doi:10.2217/fon-2016-0226
10. Catanzano AA, Kerr DL, Lazarides AL, et al. Revisiting the role of radiation therapy in chondrosarcoma: a national cancer database study. *Sarcoma*. 2019;2019:1–9. doi:10.1155/2019/4878512
11. Pagáčová E, Štefančíková L, Schmidt-Kaler F, et al. Challenges and contradictions of metal nano-particle applications for radio-sensitivity enhancement in cancer therapy. *IJMS*. 2019;20(3):588. doi:10.3390/ijms20030588
12. Kempson I. Mechanisms of nanoparticle radiosensitization. *Wiley Interdiscip Rev Nanomed Nanobiotechnol*. 2021;13(1):e1656. doi:10.1002/wnan.1656

13. Scher N, Bonvalot S, Le Tourneau C, et al. Review of clinical applications of radiation-enhancing nanoparticles. *Biotechnol Rep*. 2020;28:e00548. doi:10.1016/j.btre.2020.e00548
14. Butterworth KT, McMahon SJ, Taggart LE, Prise KM. Radiosensitization by gold nanoparticles: effective at megavoltage energies and potential role of oxidative stress. *Transl Cancer Res*. 2013;2(4). doi:10.21037/1514
15. Quatre R, Jacquet T, Atallah I, et al. Evaluation of the theranostic properties of gadolinium-based nanoparticles for head and neck cancer. *Head Neck*. 2018;hed.25460. doi:10.1002/hed.25460
16. Dufort S, Appelboom G, Verry C, et al. Ultrasmall theranostic gadolinium-based nanoparticles improve high-grade rat glioma survival. *J Clin Neurosci*. 2019;67:215–219. doi:10.1016/j.jocn.2019.05.065
17. Lux F, Tran VL, Thomas E, et al. AGuIX® from bench to bedside-Transfer of an ultrasmall theranostic gadolinium-based nanoparticle to clinical medicine. *Br J Radiol*. 2019;92(1093):20180365. doi:10.1259/bjr.20180365
18. Bort G, Lux F, Dufort S, Crémillieux Y, Verry C, Tillement O. EPR-mediated tumor targeting using ultrasmall-hybrid nanoparticles: from animal to human with theranostic AGuIX nanoparticles. *Theranostics*. 2020;10(3):1319–1331. doi:10.7150/thno.37543
19. Kotb S, Detappe A, Lux F, et al. Gadolinium-based nanoparticles and radiation therapy for multiple brain melanoma metastases: proof of concept before phase I trial. *Theranostics*. 2016;6(3):418–427. doi:10.7150/thno.14018
20. Verry C, Dufort S, Villa J, et al. Theranostic AGuIX nanoparticles as radiosensitizer: a Phase I, dose-escalation study in patients with multiple brain metastases (NANO-RAD trial). *Radiother Oncol*. 2021;160:159–165. doi:10.1016/j.radonc.2021.04.021
21. Sancey L, Lux F, Kotb S, et al. The use of theranostic gadolinium-based nanoprobes to improve radiotherapy efficacy. *Br J Radiol*. 2014;87(1041):20140134. doi:10.1259/bjr.20140134
22. Guy JB, Espenel S, Vallard A, et al. Evaluation of the cell invasion and migration process: a comparison of the video microscope-based scratch wound assay and the boyden chamber assay. *J Vis Exp*. 2017;(129). doi:10.3791/56337
23. Girard N, Lhuissier E, Aury-Landas J, et al. Heterogeneity of chondrosarcomas response to irradiations with X-rays and carbon ions: a comparative study on five cell lines. *J Bone Oncol*. 2020;22:100283. doi:10.1016/j.jbo.2020.100283
24. Perut F, Sbrana FV, Avnet S, De Milito A, Baldini N. Spheroid-based 3D cell cultures identify salinomycin as a promising drug for the treatment of chondrosarcoma. *J Orthop Res*. 2018;36:2305–2312. doi:10.1002/jor.23880
25. Monderer D, Luseau A, Bellec A, et al. New chondrosarcoma cell lines and mouse models to study the link between chondrogenesis and chemoresistance. *Lab Invest*. 2013;93(10):1100–1114. doi:10.1038/labinvest.2013.101
26. Hamdi DH, Barbieri S, Chevalier F, et al. In vitro engineering of human 3D chondrosarcoma: a preclinical model relevant for investigations of radiation quality impact. *BMC Cancer*. 2015;15(1):579. doi:10.1186/s12885-015-1590-5
27. Voissiere A, Jouberton E, Maubert E, et al. Development and characterization of a human three-dimensional chondrosarcoma culture for in vitro drug testing. *PLoS One*. 2017;12(7):e0181340. doi:10.1371/journal.pone.0181340
28. Lhuissier E, Bazille C, Aury-Landas J, et al. Identification of an easy to use 3D culture model to investigate invasion and anticancer drug response in chondrosarcomas. *BMC Cancer*. 2017;17(1):490. doi:10.1186/s12885-017-3478-z
29. Rima W, Sancey L, Aloy MT, et al. Internalization pathways into cancer cells of gadolinium-based radiosensitizing nanoparticles. *Biomaterials*. 2013;34(1):181–195. doi:10.1016/j.biomaterials.2012.09.029
30. Miladi I, Aloy MT, Armandy E, et al. Combining ultrasmall gadolinium-based nanoparticles with photon irradiation overcomes radioresistance of head and neck squamous cell carcinoma. *Nanomed Nanotechnol Biol Med*. 2015;11(1):247–257. doi:10.1016/j.nano.2014.06.013
31. Wozny AS, Aloy MT, Alphonse G, et al. Gadolinium-based nanoparticles as sensitizing agents to carbon ions in head and neck tumor cells. *Nanomed Nanotechnol Biol Med*. 2017;13(8):2655–2660. doi:10.1016/j.nano.2017.07.015
32. Štefančíková L, Lacombe S, Salado D, et al. Effect of gadolinium-based nanoparticles on nuclear DNA damage and repair in glioblastoma tumor cells. *J Nanobiotechnol*. 2016;14(1):63. doi:10.1186/s12951-016-0215-8
33. Simonet S, Rodriguez-Lafrasse C, Beal D, et al. Gadolinium-based nanoparticles can overcome the radioresistance of head and neck squamous cell carcinoma through the induction of autophagy. *J Biomed Nanotechnol*. 2020;16(1):111–124. doi:10.1166/jbn.2020.2871
34. de Jong Y, van Oosterwijk JG, Kruisselbrink AB, et al. Targeting survivin as a potential new treatment for chondrosarcoma of bone. *Oncogenesis*. 2016;5(5):e222–e222. doi:10.1038/oncsis.2016.33
35. de Jong Y, Monderer D, Brandinelli E, et al. Bcl-xl as the most promising Bcl-2 family member in targeted treatment of chondrosarcoma. *Oncogenesis*. 2018;7(9):74. doi:10.1038/s41389-018-0084-0
36. Nakagawa M, Nakatani F, Matsunaga H, et al. Selective inhibition of mutant IDH1 by DS-1001b ameliorates aberrant histone modifications and impairs tumor activity in chondrosarcoma. *Oncogene*. 2019;38(42):6835–6849. doi:10.1038/s41388-019-0929-9
37. Venneker S, Kruisselbrink AB, Briaire-de Bruijn IH, et al. Inhibition of PARP sensitizes chondrosarcoma cell lines to chemo- and radiotherapy irrespective of the IDH1 or IDH2 mutation status. *Cancers*. 2019;11(12):1918. doi:10.3390/cancers11121918
38. Qin J, Shaukat I, Mainard D, Netter P, Barré L, Ouzzine M. Constitutive activation of EGFR is associated with tumor progression and plays a prominent role in malignant phenotype of chondrosarcoma. *Oncotarget*. 2019;10(34):3166–3182. doi:10.18632/oncotarget.26899
39. Wu MH, Huang PH, Hsieh M, Tsai CH, Chen HT, Tang CH. Endothelin-1 promotes epithelial-mesenchymal transition in human chondrosarcoma cells by repressing miR-300. *Oncotarget*. 2016;7(43):70232–70246. doi:10.18632/oncotarget.11835
40. Onishi AC, Hincker AM, Lee FY. Surmounting chemotherapy and radioresistance in chondrosarcoma: molecular mechanisms and therapeutic targets. *Sarcoma*. 2011;2011:1–8. doi:10.1155/2011/381564
41. Sun X, Charbonneau C, Wei L, Yang W, Chen Q, Terek RM. CXCR4-targeted therapy inhibits VEGF expression and chondrosarcoma angiogenesis and metastasis. *Mol Cancer Ther*. 2013;12(7):1163–1170. doi:10.1158/1535-7163.MCT-12-1092
42. Giacomini A, Ghedini GC, Presta M, Ronca R. Long pentraxin 3: a novel multifaceted player in cancer. *Biochim Biophys Acta Rev Cancer*. 2018;1869(1):53–63. doi:10.1016/j.bbcan.2017.11.004
43. Kampo S, Ahmmed B, Zhou T, et al. Scorpion venom analgesic peptide, BmK AGAP inhibits stemness, and epithelial-mesenchymal transition by down-regulating PTX3 in breast cancer. *Front Oncol*. 2019;9:21. doi:10.3389/fonc.2019.00021
44. Ying TH, Lee CH, Chiou HL, et al. Knockdown of Pentraxin 3 suppresses tumorigenicity and metastasis of human cervical cancer cells. *Sci Rep*. 2016;6(1):29385. doi:10.1038/srep29385
45. Liu Q, Wang XY, Qin YY, et al. SPOCD1 promotes the proliferation and metastasis of glioma cells by up-regulating PTX3. *Am J Cancer Res*. 2018;8(4):624–635.

46. Choi B, Lee EJ, Song DH, et al. Elevated Pentraxin 3 in bone metastatic breast cancer is correlated with osteolytic function. *Oncotarget*. 2014;5 (2):481–492. doi:10.18632/oncotarget.1664
47. Song T, Wang C, Guo C, Liu Q, Zheng X. Pentraxin 3 overexpression accelerated tumor metastasis and indicated poor prognosis in hepatocellular carcinoma via driving epithelial-mesenchymal transition. *J Cancer*. 2018;9(15):2650–2658. doi:10.7150/jca.25188
48. Bonvalot S, Rutkowski PL, Thariat J, et al. NBTXR3, a first-in-class radioenhancer hafnium oxide nanoparticle, plus radiotherapy versus radiotherapy alone in patients with locally advanced soft-tissue sarcoma (Act.In.Sarc): a multicentre, phase 2–3, randomised, controlled trial. *Lancet Oncol*. 2019;20(8):1148–1159. doi:10.1016/S1470-2045(19)30326-2